

pubs.acs.org/JPCL Letter

# Quantum Coupling of Two Atomic Defects in a Carbon Nanotube **Semiconductor**

Jacob Fortner and YuHuang Wang\*



Cite This: J. Phys. Chem. Lett. 2022, 13, 8908-8913



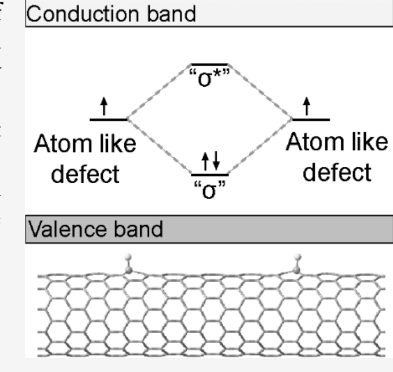
ACCESS I

Metrics & More

Article Recommendations

Supporting Information

ABSTRACT: Chemical defects can create organic color centers in the graphitic lattice of single-walled carbon nanotubes. However, the underlying physics remains somewhat of a mystery. Here we show that two sp<sup>3</sup> atomic defects can interact with each other in a way reminiscent of atoms bonding to form molecules. Each defect creates an atom-like mid-gap state within the band gap of the nanotube semiconductor. Two such defects, when brought close to each other, interact to form a split pair of orbitals akin to two hydrogen atoms covalently bonding to form a H2 molecule. This unexpected finding may help in understanding the nature of atomic defects in solids and provide a fresh perspective to the engineering of these color centers.



rganic color centers (OCCs) are fluorescent quantum defects that can be created in single-walled carbon nanotubes (SWCNTs) by the covalent attachment of functional groups to the nanotube sidewall. The functionalization converts the sp<sup>2</sup> carbons into sp<sup>3</sup> defects within the carbon nanotube lattice. Several different chemistries have been utilized to create these atomic defects, including aryldiazonium chemistry,<sup>2</sup> reductive alkylation,<sup>3</sup> photochemical reaction of aryl compounds, 4,5 and singlet oxygen activation of guanine nucleotides in DNA.6 The photoluminescence from OCCs is distinctly different from the intrinsic photoluminescence of the nanotube host. OCCs emit in the short-wave infrared with high quantum yield,2 selectively respond to changes in the microenvironment near the OCC,<sup>7</sup> and exhibit high singlephoton purity at room temperature.8 These properties give OCC many potential applications in fields such as quantum photonics, chemical sensing, 7,10,11 and bioimaging. 12 All current OCCs feature either a pair of defects or a single sp<sup>3</sup> defect paired with a radical.

DFT calculations predict for an OCC comprised of a pair of sp<sup>3</sup> defects the bonding configuration (relative positions between the two defects on the SWCNT surface) has a large impact on the defect photoluminescence. 13,14 These previous studies predominately focused on the closest possible configurations of these two defects that can arise where the defects are separated by either one carbon-carbon bond (ortho configurations) or three carbon-carbon bonds (para configurations) on the SWCNT surface. However, the underlying nature of how the two sp<sup>3</sup> defects interact to enable the fluorescence from the OCC and how this relates to the single sp<sup>3</sup> defect is not well understood. In this work we

utilize density functional theory (DFT) to study the interaction of two sp<sup>3</sup> defects in a SWCNT. By tracing the orbital and orbital energy changes as the two sp<sup>3</sup> defects move from isolated states (5 nm apart) to the limit of strong coupling (a single C-C bond separation), we show that new defect photoluminescence may arise from two sp<sup>3</sup> defects interacting at a much larger distance.

On a cylindrical surface, the distance between two point defects depends on both the axial displacement (how far apart they are along the length of the cylinder) and the angular displacement (how far apart they are around the circumference of the cylinder). For a pair of sp<sup>3</sup> defects in SWCNTs, these two parameters are typically correlated because the two defect carbon atoms must fit into the underlying graphitic lattice of the nanotube sidewall. In this study, we focus on (11,0) as the model system due to its mirror symmetry along the SWCNT axis, which allows for axial distances between two sp<sup>3</sup> defects to be chosen independently of the angular displacement. Additionally, (6,5) is used as a comparison as it has been heavily studied in the literature, both experimentally and theoretically. <sup>2,3,14</sup> This near armchair chirality SWCNT lacks mirror symmetry in the underlying graphitic lattice, which intrinsically couples the effects of axial and angular displacements between the two defects.

Received: August 5, 2022 Accepted: September 15, 2022 Published: September 20, 2022





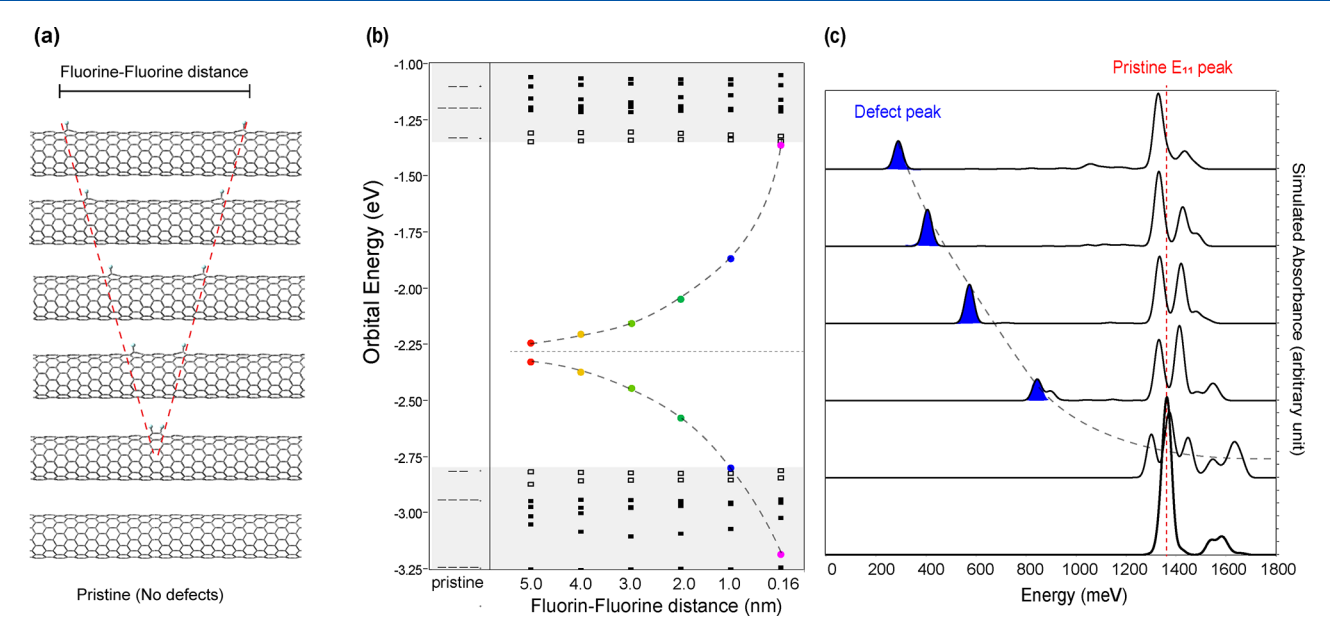


Figure 1. Coupling of two atomic defects on a carbon nanotube lattice. (a) Models of two fluorine defects on a (11,0)-SWCNT with the defect-defect spacing decreased from 5 nm to a single C–C bond distance. (b) Molecular orbital energy diagrams showing the defects create a pair of midgap orbitals with an energy splitting that increases when the defects are brought closer. Dashed lines show the boundary between the occupied and unoccupied orbitals for the ground state. Shaded areas at the top and bottom represent the energy state continuum of the conduction and valence bands, respectively. Black squares indicate pristine-like orbitals, with the empty squares denoting the orbitals split band gap states in the presence of defects. Colored circles indicate new pseudo diatomic molecular defect states associated with the OCC. The dashed lines are included to emphasize the increased splitting of the defect states with decreasing defect—defect separation. (c) Simulated absorbance spectra showing the first 50 singlet excited state transitions at each defect—defect distance. Transition peak positions and oscillator strengths were calculated using TD-DFT and the absorption spectra were created assuming a Gaussian peak shape and fwhm of 25 meV. The peaks resulting from the transition exclusively between the two new defect states are shaded in blue. Compared to the pristine SWCNT, the addition of the defects creates a new pair of orbitals while splitting the degenerate pristine orbitals. The energy gap between these two new states is larger when the defects are closer together. When the defects are separated by a single C–C bond in the SWCNT, the new orbitals are located outside of the pristine band gap.

We modeled the (11,0) SWCNT either as infinitely long by using 1D periodic boundary conditions with a  $\sim$ 10 nm long supercell (equivalent to 23 pristine (11,0) unit cells) or using  $\sim$ 10 nm finite length with the end carbons terminated by a combination of seven hydrogens and four methylenes at each end. The methylene groups effectively reduce the effects of the ends of the nanotube, as previously observed by Kilina and Trietiak. The (6,5) SWCNT models were infinitely long with  $\sim$ 8 nm long supercell (equivalent to two pristine (6,5) unit cells). For the infinitely long models, the periodic unit cell size was chosen to limit the interaction between the defects across the cell boundary while still maintaining a reasonable system size for quantum chemical calculations.

The defects studied include a single fluorine, a pair of fluorines, and an aryl hydroxyl pair ( $C_6H_5+OH$ ) that are covalently attached to the SWCNT surface. The fluorine atoms are among the simplest type of defect functional groups, while the  $C_6H_5+OH$  pair defect represents the typical type of defects experimentally attainable through diazonium chemistry.  $^{2,16}$ 

When the defect functional group is covalently attached to the SWCNT surface, the carbon atom to which it is attached is converted from  $\mathrm{sp^2}$  hybridization, which takes on a trigonal planar shape, to  $\mathrm{sp^3}$  hybridization that wants to have a tetrahedral shape; as such, the defect group will not point straight up from the SWCNT surface but will instead tilt at an angle. For (11,0), this tilt will be in the direction of the nanotube axis. If we view the SWCNT from the side, the SWCNT  $\rightarrow$  defect bond will tilt either to the right or to the left, which means that for each pair of defects there are four

possible alignments:  $[\leftarrow,\leftarrow]$ ,  $[\leftarrow,\rightarrow]$ ,  $[\rightarrow,\leftarrow]$ , and  $[\rightarrow,\rightarrow]$ . Due to the mirror symmetry of the (11,0) SWCNT, the  $[\leftarrow,\leftarrow]$  and  $[\rightarrow,\rightarrow]$  alignments are identical, leaving us with only three unique alignments. For simplicity in this work all defect pairs are arranged in the  $[\leftarrow,\rightarrow]$  alignment  $(C\rightarrow F)$  bonds tilting away from each other).

For the defect pairs, six different spacings between the defects were compared. For (11,0), we started with the defects separated by a single C-C bond along the SWCNT axis (referred to as the "Ortho +" configuration in the liturature 13). The remaining models were created by moving both defect groups away from the center in step sizes of four carbon bonds (for a total of eight carbon bond additional separation between the two defects) down the SWCNT axis, up to a maximum separation of ~4.8 nm, Figure S1a in the Supporting Information. Due to the mirror symmetry of the (11,0), these specific step sizes allow the two defects to align along the tubular axis without any angular displacement. For the (6,5) model, a similar step size was used, but there is some angular displacement due to the intrinsic coupling of angular and axial displacement that occurs from the chiral twist, which breaks the mirror symmetry, as shown by Figure S1b in the Supporting Information.

The SWCNTs models were built using the nanotube generator included with the Avogadro software package <sup>17</sup> and then the defects were added using Gaussview (version 6.0.16). <sup>18</sup> All DFT calculations were performed using the Gaussian09 software package (version E.01) <sup>19</sup> and visualized using Gaussview. <sup>18</sup> Geometry optimization was performed for all models using the B3LYP/STO-3G level of theory. We note

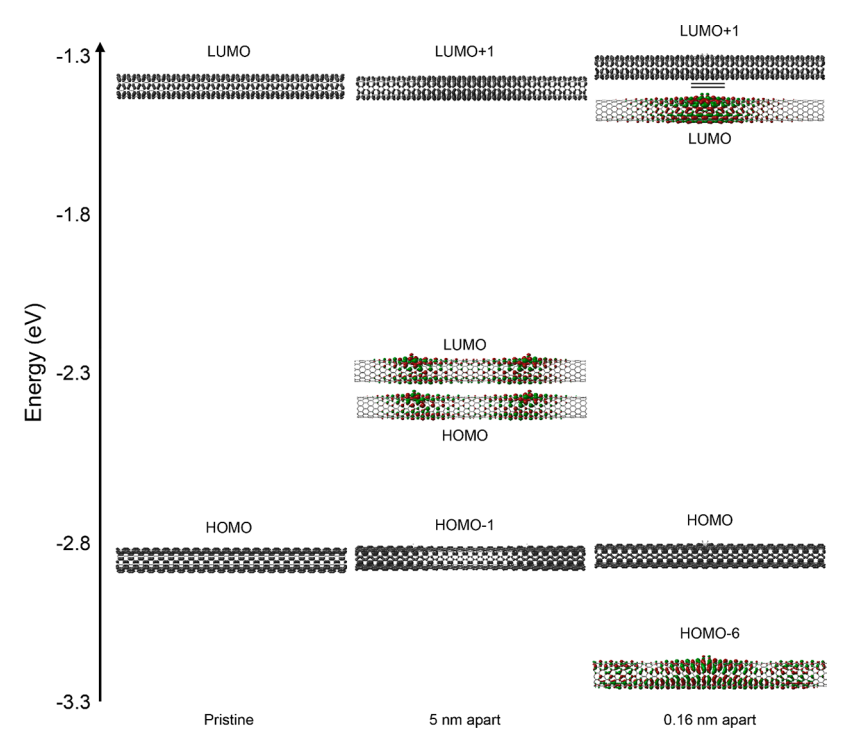


**Figure 2.** Coupling of two sp<sup>3</sup> defects forms new orbitals without significantly interacting with the pristine SWCNT orbitals. Frontier orbitals (isovalue = 0.005) for (11,0) SWCNT that are pristine (left), with the addition of two fluorine defects separated at the weak-interacting distance of 5 nm (middle), and with the addition of two fluorines separated by 0.16 nm (single C–C bond) (bottom). The models are arranged by the energy level, with the exception of the LUMO and LUMO+1 for the 0.16 nm separation where the actual energy levels are denoted by the two black lines between the two models. For the pristine tube, the HOMO and LUMO are uniformly distributed along the length (outside of a small perturbation at the unit cell boundary) and have a clear periodic structure. With the addition of the defects 5 nm apart, the HOMO and LUMO are localized around the defects on the SWCNT surface; meanwhile, the HOMO-1 and LUMO+1 maintain the delocalized and periodic structures as with the HOMO and LUMO from the pristine tube, only with some variation in the density near the defects. When the defects are separated by 0.16 nm (single C–C bond), the HOMO and LUMO+1 are nearly identical to the HOMO and LUMO of the pristine SWCNT; meanwhile, the HOMO-6 and LUMO orbitals show strong localization around the defects, indicating they are the new orbitals added by the defects.

that while range-separated functionals are known to provide more quantitatively accurate results for the electronic properties of SWCNTs and other conjugated systems than B3LYP, <sup>20,21</sup> it has been shown that B3LYP provides qualitatively accurate results for modeling SWCNT optical properties comparable with the results from the range-separated CAM-B3LYP functional. <sup>14,22</sup>

The models with a single fluorine defect were neutral charge open-shell systems, and the optimizations were performed using the unrestricted open-shell B3LYP functional. For the finite length (11,0) models, the geometry optimization was followed by time-dependent density functional theory (TD-DFT) calculations (using the same functional/basis set as that used for the optimization) to find the first 50 singlet excited state transitions. To demonstrate that the observed defect coupling behavior is not an artifact due to the use of a limited basis set size or spurious long-range interactions, additional optimization and TD-DFT calculations were performed as controls at the B3LYP-D3/3-21G level of theory for the models with two fluorine defects in finite length (11,0) and separations of 4 and 2 nm, and a single C–C bond (see Figures S2 and S3 in the Supporting Information).

Starting from a pristine SWCNT model, two fluorine atoms were covalently bonded to the nanotube surface to form a pair of sp<sup>3</sup> defects at increasing distances, Figure 1a. When the two defects were far apart from each other, we observed two new states within the band gap of the SWCNT semiconductor, including a fully occupied lower energy state and an

unoccupied higher energy state, Figure 1b. These two new states differ by 85 meV in energy when the two defects are separated by 5 nm (10 units cells). However, as the defects were moved closer together in step sizes of 1 nm (two unit cells), the energy difference between these two states increased, reaching 927 meV at 1 nm (Figure 1b). When the fluorine defects were separated only by a single C–C bond (0.16 nm), the lower defect energy state had dropped below the edge of the valence band and the higher defect energy state became comparable in energy to the band edge states of the conduction band.

This behavior is not exclusive to fluorine radical defects in (11,0) SWCNT but occurs in all of the other defects and nanotube chiralities studied here. The same trend of energy level splitting was observed when an aryl  $(-C_6H_5)$  and hydroxyl (-OH) pair is in place of the two F atoms (see Figure S4a in the Supporting Information). While the energy levels associated with the mid-gap states of the aryl + hydroxyl pair are ~100 meV higher in energy compared to the defects composed of two F atoms, the same trend holds. If the highly symmetric (11,0) SWCNT is replaced with the lower symmetry (6,5), a similar type of energy splitting is still found (see Figure S4b in the Supporting Information). We note that while the energy splitting of the defects increases smoothly as the defects are brought closer together in (11,0) SWCNT, in (6,5) the energy splitting includes a stepwise component which is likely due to the additional angular displacement of the defects in the (6,5), as opposed to the

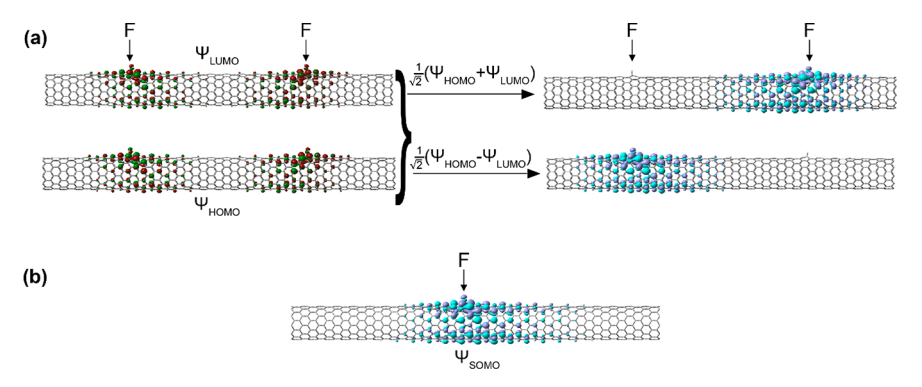


Figure 3. Frontier orbitals of an OCC are a linear combination of two SOMOs. (a) Orbital arithmetic of (11,0) SWCNT with two fluorines separated by 5 nm. The HOMO and LUMO are equally localized around both defects. The symmetric and antisymmetric combination of the HOMO and LUMO results in a new pair of orbitals where each is localized around only one defect and has the same shape as the SOMO of a SWCNT tailored with one single defect, indicating that the HOMO and LUMO are made of the symmetric and antisymmetric combinations of the individual fluorine radical defect orbitals. (b) SOMO for a model with a single fluorine radical defect, for comparison with the symmetric and antisymmetric addition orbitals. For all of the panels, the isovalue = 0.01.

strictly axial displacement used in the (11,0). However, in both cases, as the defects get closer together, the energy splitting between the defect states increases. Because this trend did not significantly change regardless of the functional group used or the chirality of the host SWCNT, this behavior is likely generalizable to other sp<sup>3</sup> defect systems.

To verify whether there are optically allowed transitions between these defect states, we performed TD-DFT calculations to find the first 50 optical allowed singlet state transitions. For the case where the two defects are separated by a single C–C bond, our model is in agreement with previous DFT studies on the Ortho + configuration, in which the OCC creates defect PL red-shifted by ~40 meV from the pristine nanotube emission due to the splitting of the pristine band edge states.<sup>23</sup>

However, for all models where the fluorine defects were separated by 1 nm or more, the simulated absorption spectra show two new sets of lower energy peaks when compared to the simulated absorption spectrum of the pristine (11,0) SWCNT, Figure 1c. In addition to the OCC transition that occurs at the energy vicinity of the E<sub>11</sub> excitonic transition of the nanotube host, we observed a distinctly different peak that blue shifts as the two sp<sup>3</sup> defects are moved closer. This result differs from OCC photoluminescence in which the defects perturb and split the existing degenerate band edge states, resulting in a narrowing of the band gap at the defect site. 24,25 This behavior is also different from what was found in a previous study by Weight et al.,26 which studied the coupling behavior of two OCCs, where each OCC is made of a pair of sp<sup>3</sup> defects separated by either one or three carbon bonds (resulting in a total of four sp<sup>3</sup> defects, rather than a pair of sp<sup>3</sup> defects considered in our work). In that work, it was shown that when two defect pairs are moved closer, the defect emission energy shifts to the red. By contrast, our present work modeling the interaction of two sp<sup>3</sup> defects shows a blue shift in emission energy as the defects are moved closer. This suggests that interactions between multiple OCCs are governed by a different mechanism than the interactions between two individual sp<sup>3</sup> defects and a new type of optical transition is at play here. As we will discuss in the following sections, this new optical transition can be attributed to the coupling of defect-induced mid-gap singly occupied molecular orbitals (SOMOs), with optical signature distinctly different from the OCC PL reported previously by us and others.<sup>2,3,5,8,27</sup>

We first identified the orbitals associated with the defect pair by examining the Khon-Sham orbitals for each energy state. For all models where the defects were separated by 1 nm or more, the two new states within the pristine band gap were the highest occupied molecular orbital (HOMO) and lowest unoccupied molecular orbital (LUMO) and were both highly localized around the defects. At the same time the second highest occupied orbital (HOMO-1) and second lowest unoccupied orbital (LUMO+1) were delocalized and similar in energy to the HOMO and LUMO of the pristine SWCNT (Figure 2).

In the case when the two defects are separated by a single C-C bond, the new orbitals localized near the defects are the LUMO and HOMO-6, while the HOMO through HOMO-5 still maintain a similar shape to the corresponding orbitals of a pristine SWCNT (see Figure S5 in the Supporting Information). Note that for the closest defect spacing (separated by a single C-C bond), the two "mid-gap state" orbitals fall outside of the nanotube band gap and we were not able to identify a higher energy optical transition that could be clearly attributed to the transition between the two defect states. This may be due to orbital mixing, as the lower defect energy state now has an energy similar to several of the valence band states, or it could simply be that the coupled defect transition has an energy larger than the 50 lowest energy excited states.

This orbital analysis suggests that the defects introduce entirely new states into the system that are different from the states due to the defect-induced splitting of the doubly degenerate frontier orbitals of the nanotube host. These new states originate from the defect-induced mid-gap states which are SOMOs in nature. This origin is further supported by symmetry analysis of the orbitals. We observed that the symmetric and antisymmetric combinations of the two defect orbitals are entirely localized around only one or the other of the two defects, approximating the orbitals of two isolated, defect-induced SOMOs (Figure 3). The orbitals of the coupled defect pair can be broken down as the symmetric and antisymmetric combination of the two SOMOs and display the following relation:

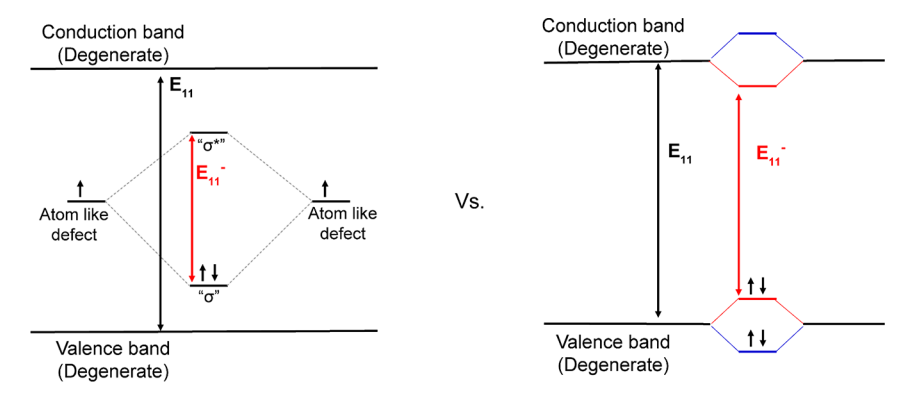


Figure 4. "Bonding" model of two coupled atomic defects in a solid. Two radical atomic defects with mid-gap energy state in a semiconductor interact to form a pseudo diatomic bond between the defects, similar to two hydrogens atomic orbitals interacting to form the bonding and antibonding orbitals of an  $H_2$  molecule. This bonding model contrasts with the OCC model (right), where the presence of the defects splits the degenerate band edge states of the SWCNT, resulting in a narrower band gap at the defect site.

$$\begin{cases} \frac{1}{\sqrt{2}}(\psi_{A} + \psi_{B}) = \psi_{A'} \\ \frac{1}{\sqrt{2}}(\psi_{A} - \psi_{B}) = \psi_{B'} \end{cases} \rightarrow \begin{cases} \frac{1}{\sqrt{2}}(\psi_{A'} + \psi_{B'}) = \psi_{A} \\ \frac{1}{\sqrt{2}}(\psi_{A'} - \psi_{B'}) = \psi_{B} \end{cases}$$

Strikingly, this relation resembles how two degenerate atomic hydrogen orbitals combine to form the bonding and antibonding orbitals of molecular hydrogen. This similarity suggests that two atomic defects could interact in a way that may be simply pictured, at least to some degrees, akin to two reactive atoms, albeit in a solid.

In Figure 4 we plot this "bonding" picture in contrast with the frontier orbital splitting mechanism. Our results suggest that in addition to splitting the doubly degenerated frontier orbitals of the nanotube as proposed previously, 24,28 these atomic defects introduce two entirely new states that are SOMOs in nature when isolated. Both types of "defect" orbitals (coupled radical orbital and splitting of the degenerate band edge orbital) are found to exist regardless of the distance between the radical defects. The SOMOs defect states can couple, even at a defect-defect distance as large as 5 nm, to create new states that fall within the pristine band gap. As the transition between the coupled mid-gap states is optically active and increasing the distance between the defects can result in optical transitions much lower in energy than the pristine SWCNT transition, this suggest the possibility that these states could be a source of the OCC emission peaks observed experimentally under certain conditions and that the defect PL may occur under different mechanisms depending on the distance between the two sp<sup>3</sup> defects that make up the OCC.

In conclusion, we conducted DFT calculations to investigate the origin of defect PL in SWCNTs and our results predict an optical signature due to quantum coupling of two sp³ defects at distances well beyond the ortho and para configurations. Each defect creates a localized mid-gap state in the nanotube semiconductor. Through analysis of the molecular orbitals and the trend in energy spacing, we found two individual sp³ defects can couple to form a pair of pseudo diatomic molecular orbitals and an optically active transition between them, with the transition energy increasing with smaller defect—defect distance, extending beyond the band gap of the nanotube at the shortest distance (a single C–C bond). Our results suggest that in addition to the orbital splitting mechanism that gives

rise to the experimentally observed OCC fluorescence, individual sp<sup>3</sup> defects in a SWCNT may couple at significantly larger distances to create pseudo diatomic molecular transitions that can fall within the band gap.

#### ASSOCIATED CONTENT

#### Supporting Information

The Supporting Information is available free of charge at https://pubs.acs.org/doi/10.1021/acs.jpclett.2c02439.

Defect spacing scheme diagram, effect of of increasing the basis set size and including long range disspersion corrections, orbital energy diagrams for additional SWCNT models, and identification of defect orbitals outside the band gap (PDF)

#### AUTHOR INFORMATION

## **Corresponding Author**

YuHuang Wang — Chemical Physics Program, University of Maryland, College Park, Maryland 20742, United States; Department of Chemistry and Biochemistry, University of Maryland, College Park, Maryland 20742, United States; orcid.org/0000-0002-5664-1849; Email: yhw@umd.edu

#### Author

Jacob Fortner — Chemical Physics Program, University of Maryland, College Park, Maryland 20742, United States; Department of Chemistry and Biochemistry, University of Maryland, College Park, Maryland 20742, United States; orcid.org/0000-0002-2379-0151

Complete contact information is available at: https://pubs.acs.org/10.1021/acs.jpclett.2c02439

#### Notes

The authors declare no competing financial interest.

#### ACKNOWLEDGMENTS

We gratefully acknowledge the National Science Foundation (Grant No. CHE2204202) for partial support of this work. We thank Jacek Klos and Sergei Tretiak for valuable discussions.

### REFERENCES

(1) Brozena, A. H.; Kim, M.; Powell, L. R.; Wang, Y. Controlling the Optical Properties of Carbon Nanotubes with Organic Colour-Centre Quantum Defects. *Nat. Rev. Chem.* **2019**, *3*, 375–392.

- (2) Piao, Y.; Meany, B.; Powell, L. R.; Valley, N.; Kwon, H.; Schatz, G. C.; Wang, Y. Brightening of Carbon Nanotube Photoluminescence through the Incorporation of sp3 Defects. *Nat. Chem.* **2013**, *5*, 840–845.
- (3) Kwon, H.; Furmanchuk, A.; Kim, M.; Meany, B.; Guo, Y.; Schatz, G. C.; Wang, Y. Molecularly Tunable Fluorescent Quantum Defects. J. Am. Chem. Soc. 2016, 138, 6878–6885.
- (4) Wu, X.; Kim, M.; Kwon, H.; Wang, Y. Photochemical Creation of Fluorescent Quantum Defects in Semiconducting Carbon Nanotube Hosts. *Angew. Chem., Int. Ed. Engl.* **2018**, *57*, 648–653.
- (5) Zheng, Y.; Bachilo, S. M.; Weisman, R. B. Photoexcited Aromatic Reactants Give Multicolor Carbon Nanotube Fluorescence from Quantum Defects. ACS Nano 2020, 14, 715–723.
- (6) Zheng, Y.; Bachilo, S. M.; Weisman, R. B. Controlled Patterning of Carbon Nanotube Energy Levels by Covalent DNA Functionalization. *ACS Nano* **2019**, *13*, 8222–8228.
- (7) Kwon, H.; Kim, M.; Meany, B.; Piao, Y.; Powell, L. R.; Wang, Y. Optical Probing of Local pH and Temperature in Complex Fluids with Covalently Functionalized, Semiconducting Carbon Nanotubes. *J. Phys. Chem. C* **2015**, *119*, 3733–3739.
- (8) He, X.; Hartmann, N. F.; Ma, X.; Kim, Y.; Ihly, R.; Blackburn, J. L.; Gao, W.; Kono, J.; Yomogida, Y.; Hirano, A.; et al. Tunable Room-Temperature Single-Photon Emission at Telecom Wavelengths from sp3 Defects in Carbon Nanotubes. *Nat. Photonics* **2017**, *11*, 577–582.
- (9) Luo, Y.; He, X.; Kim, Y.; Blackburn, J. L.; Doorn, S. K.; Htoon, H.; Strauf, S. Carbon Nanotube Color Centers in Plasmonic Nanocavities: A Path to Photon Indistinguishability at Telecom Bands. *Nano Lett.* **2019**, *19*, 9037–9044.
- (10) Shiraki, T.; Onitsuka, H.; Shiraishi, T.; Nakashima, N. Near Infrared Photoluminescence Modulation of Single-Walled Carbon Nanotubes Based on a Molecular Recognition Approach. *Chem. Commun.* **2016**, *52*, 12972–12975.
- (11) Onitsuka, H.; Fujigaya, T.; Nakashima, N.; Shiraki, T. Control of the Near Infrared Photoluminescence of Locally Functionalized Single-Walled Carbon Nanotubes via Doping by Azacrown-Ether Modification. *Chem. Eur. J.* **2018**, *24*, 9393–9398.
- (12) Mandal, A. K.; Wu, X.; Ferreira, J. S.; Kim, M.; Powell, L. R.; Kwon, H.; Groc, L.; Wang, Y.; Cognet, L. Fluorescent sp3 Defect-Tailored Carbon Nanotubes Enable NIR-II Single Particle Imaging in Live Brain Slices at Ultra-Low Excitation Doses. *Sci. Rep.* **2020**, *10*, 5286.
- (13) Saha, A.; Gifford, B. J.; He, X.; Ao, G.; Zheng, M.; Kataura, H.; Htoon, H.; Kilina, S.; Tretiak, S.; Doorn, S. K. Narrow-Band Single-Photon Emission through Selective Aryl Functionalization of Zigzag Carbon Nanotubes. *Nat. Chem.* **2018**, *10*, 1089–1095.
- (14) He, X.; Gifford, B. J.; Hartmann, N. F.; Ihly, R.; Ma, X.; Kilina, S. V.; Luo, Y.; Shayan, K.; Strauf, S.; Blackburn, J. L.; et al. Low-Temperature Single Carbon Nanotube Spectroscopy of sp3 Quantum Defects. *ACS Nano* **2017**, *11*, 10785–10796.
- (15) Kilina, S.; Tretiak, S. Excitonic and Vibrational Properties of Single-Walled Semiconducting Carbon Nanotubes. *Adv. Funct. Mater.* **2007**, *17*, 3405–3420.
- (16) Wang, P.; Fortner, J.; Luo, H.; Kłos, J.; Wu, X.; Qu, H.; Chen, F.; Li, Y.; Wang, Y. Quantum Defects: What Pairs with the Aryl Group When Bonding to the sp2 Carbon Lattice of Single-Wall Carbon Nanotubes? J. Am. Chem. Soc. 2022, 144, 13234–13241.
- (17) Hanwell, M. D.; Curtis, D. E.; Lonie, D. C.; Vandermeersch, T.; Zurek, E.; Hutchison, G. R. Avogadro: An Advanced Semantic Chemical Editor, Visualization, and Analysis Platform. *J. Cheminf.* **2012**, *4*, 17.
- (18) Dennington, R.; Keith, T. A.; Millam, J. M. Gaussview, 6.0.16; Semichem: Shawnee Mission, KS, USA, 2016.
- (19) Frisch, M. J.; Trucks, G. W.; Schlegel, H. B.; Scuseria, G. E.; Robb, M. A.; Cheeseman, J. R.; Scalmani, G.; Barone, V.; Petersson, G. A.; Nakatsuji, H.; et al. *Gaussian 09*, Rev. E.01; Gaussian: Wallingford, CT, USA, 2013.
- (20) Zhou, B.; Hu, Z.; Jiang, Y.; He, X.; Sun, Z.; Sun, H. Benchmark Study of Ionization Potentials and Electron Affinities of Armchair

- Single-Walled Carbon Nanotubes Using Density Functional Theory. *J. Phys.: Cond. Matter* **2018**, *30*, 215501.
- (21) Wong, B. M.; Hsieh, T. H. Optoelectronic and Excitonic Properties of Oligoacenes: Substantial Improvements from Range-Separated Time-Dependent Density Functional Theory. *J. Chem. Theory Comp.* **2010**, *6*, 3704–3712.
- (22) Gifford, B. J.; Sifain, A. E.; Htoon, H.; Doorn, S. K.; Kilina, S.; Tretiak, S. Correction Scheme for Comparison of Computed and Experimental Optical Transition Energies in Functionalized Single-Walled Carbon Nanotubes. *J. Phys. Chem. Lett.* **2018**, *9*, 2460–2468.
- (23) Gifford, B. J.; Saha, A.; Weight, B. M.; He, X.; Ao, G.; Zheng, M.; Htoon, H.; Kilina, S.; Doorn, S. K.; Tretiak, S. Mod(n-m,3) Dependence of Defect-State Emission Bands in Aryl-Functionalized Carbon Nanotubes. *Nano Lett.* **2019**, *19*, 8503–8509.
- (24) Ghosh, S.; Bachilo, S. M.; Simonette, R. A.; Beckingham, K. M.; Weisman, R. B. Oxygen Doping Modifies Near-Infrared Band Gaps in Fluorescent Single-Walled Carbon Nanotubes. *Science* **2010**, 330, 1656–1659.
- (25) Shiraki, T.; Miyauchi, Y.; Matsuda, K.; Nakashima, N. Carbon Nanotube Photoluminescence Modulation by Local Chemical and Supramolecular Chemical Functionalization. *Acc. Chem. Res.* **2020**, *53*, 1846–1859.
- (26) Weight, B. M.; Sifain, A. E.; Gifford, B. J.; Kilin, D.; Kilina, S.; Tretiak, S. Coupling between Emissive Defects on Carbon Nanotubes: Modeling Insights. *J. Phys. Chem. Lett.* **2021**, *12*, 7846–7853.
- (27) Settele, S.; Berger, F. J.; Lindenthal, S.; Zhao, S.; El Yumin, A. A.; Zorn, N. F.; Asyuda, A.; Zharnikov, M.; Högele, A.; Zaumseil, J. Synthetic Control over the Binding Configuration of Luminescent sp3 Defects in Single-Walled Carbon Nanotubes. *Nat. Commun.* **2021**, *12*, 2119.
- (28) Kilina, S.; Ramirez, J.; Tretiak, S. Brightening of the Lowest Exciton in Carbon Nanotubes via Chemical Functionalization. *Nano Lett.* **2012**, *12*, 2306–2312.

## **□** Recommended by ACS

#### On-the-Fly Nonadiabatic Dynamics Simulations of Single-Walled Carbon Nanotubes with Covalent Defects

Braden M. Weight, Sergei Tretiak, et al.

MARCH 27, 2023

ACS NANO

READ 🗹

#### Signatures of Chemical Dopants in Simulated Resonance Raman Spectroscopy of Carbon Nanotubes

Braden M. Weight, Sergei Tretiak, et al.

JANUARY 30, 2023

THE JOURNAL OF PHYSICAL CHEMISTRY LETTERS  $\,$ 

READ 🗹

Broadband Full-Spectrum Raman Excitation Mapping Reveals Intricate Optoelectronic-Vibrational Resonance Structure of Chirality-Pure Single-Walled Carbon Nanot...

Paul Finnie, Jeffrey A. Fagan, et al.

APRIL 03, 2023

ACS NANO

READ [7

#### Room Temperature Lasing from Semiconducting Single-Walled Carbon Nanotubes

Jia-Shiang Chen, Xuedan Ma, et al.

SEPTEMBER 19, 2022

ACS NANO

READ 🗹

Get More Suggestions >